ChemPubSoc Europe

DOI: 10.1002/cphc.201700252

CHEMPHYSCHEM Articles

Noncovalent Interactions between Dopamine and Regular and Defective Graphene

Ana C. Rossi Fernández and Norberto J. Castellani*[a]

The role of noncovalent interactions in the adsorption of biological molecules on graphene is a subject of fundamental interest regarding the use of graphene as a material for sensing and drug delivery. The adsorption of dopamine on regular graphene and graphene with monovacancies (GV) is theoretically studied within the framework of density functional theory. Several adsorption modes are considered, and notably those in which the dopamine molecule is oriented parallel or quasi-parallel to the surface are the more stable. The adsorption of dopamine on graphene implies an attractive interaction of a dispersive nature that competes with Pauli repulsion between the occupied π orbitals of the dopamine ring and the π orbitals of graphene. If dopamine adsorbs at the monovacancy in the A–B stacking mode, a hydrogen bond is produced between one of the dopamine hydroxy groups and one carbon atom around the vacancy. The electronic charge redistribution due to adsorption is consistent with an electronic drift from the graphene or GV surface to the dopamine molecule.

1. Introduction

One of the main objectives of nanotechnology is to achieve the transduction of information at the molecular level by means of electronic devices of nanoscopic size. This objective is well exemplified by the interest of researchers in detecting molecules at very low concentrations. Recently, this has been addressed by using carbonaceous systems with conjugated sp^2 C–C bonds[1] in the form of one-dimensional arrays such as carbon nanotubes (CNTs) and two-dimensional arrays such as graphene. In contrast, graphene shows impressive electron-transport properties as a semi-metallic material and an extremely high surface-to-volume ratio, making it suitable in applications as a sensor of molecules. The interaction of electron-donor and electron-acceptor molecules with graphene is the basis for modifying the electronic properties of this material. The measurement of resistivity variations due to changes in the type and density of charge carriers in graphene under direct current fields allowed the ultimate single-molecule sensitivity for CO, H_2O, NO_2 and NH_3 to be attained.[2] The ability to fine tune the electrical conductivity by in graphene field-effect transistor (FET) devices make them extremely sensitive sensors of biological molecules. In the so-called Bio-FET, the charge transfer from an adsorbed molecule to the gate causes a shift in the Dirac point and consequently a change in the measured resistance, thus modifying the transconductance of the gate.[3] Recently, the fluorescence-quenching properties of graphene have been used in the selective detection of biomolecules. It was observed that the intermolecular p-orbital overlaps between graphene and fluorescent molecules of aromatic structure is associated with a photon-induced electron transfer process that leads to fluorescence quenching.[4] Moreover, graphene oxide was found to strongly interact with amino acids such as tryptophan and tyrosine, peptides and proteins, giving rise to fluorescence quenching.[5] In another approach to sensing analytes, graphene has been used as an electrode material in electrochemical sensors. It is known that the electron-transfer rates for metal cations at a graphene electrode are several orders of magnitude higher than those at glassy carbon electrodes.[6] Graphene showed excellent performance in the direct electrochemistry of enzymes, the electrochemical detection of small biomolecules, and electroanalysis.[7,8]

The transduction and recognition of an analyte molecule can be accomplished by its direct adsorption on graphene or by the functionalization of a graphene surface by attachment of appropriate biorecognition elements such as antibodies, DNA, or peptides. In both cases, the anchoring of the analyte molecule or the molecular probe to graphene can be covalent or noncovalent. Whereas covalent linking of the graphene necessarily disrupts its sp^2 structure, thereby altering its electronic properties, noncovalent linking does not present this disadvantage. In any case, the analyte molecule or the biomolecular probe must be stably bonded to the gate during measurements, a requirement that is satisfied by adsorbing aromatic molecules or polypeptides which can align with the graphene lattice.[3] A way to improve the anchoring of a chemical species to graphene is by the production of defects in the graphene lattice, such as substitutional atoms or carbon monovacancies. Recently, it was theoretically shown that the adsorption of molecules such as CO, NO, NO_2 or NH_3 on graphene containing monovacancies is a much more reactive process than the ad-

[a] A. C. R. Fernández, Prof. Dr. N. J. Castellani
IFISUR, Universidad Nacional del Sur, CONICET
Departamento de Física
Av. L. N. Alem 1253, B8000CPB Bahía Blanca (Argentina)
E-mail: castella@criba.edu.ar

Supporting Information and the ORCID identification number(s) for the author(s) of this article can be found under: https://doi.org/10.1002/cphc.201700252.

sorption graphene substitutionally doped with B, N, or P atoms.[9]

The biological molecule dopamine (DA) is an important neurotransmitter that plays a significant role in the function of the mammalian central nervous, renal and hormonal systems.[10] Low or high levels of DA are related to serious human neural diseases, such as Parkinson's disease and schizophrenia, respectively.[11] The detection of DA performed using voltammetric techniques with graphene electrodes has been a subject of increasing interest, taking into account that DA is an electrochemically active compound through the oxidation of DA phenolic hydroxy groups to give *o*-dopamine-quinone.[12–14] A high level of sensitivity was obtained using so-called solution-gated graphene transistors, whereby the graphene channel is in contact with an electrolyte instead of the gate insulator.[15] The detection of DA was reported also[16] using a fluorescence technique and a fluorescein isothiocyanate conjugate of graphene oxide as a novel supporting matrix for DA.

The noncovalent interaction between aromatic molecules and graphene can be attributed, by making an analogy to arene systems and other complexes having phenyl rings, to the presence of so-called π–π stacking. In this type of interaction, which has been recognized as a key stabilizing force in supramolecular chemistry, crystal engineering and molecular biology, the species involved arrange in a parallel manner. In π–π stacking, the π orbitals do not behave as in conventional overlap-driven covalent bonding. Instead, a careful account of nonlocal electron correlation effects must be performed.[17] Recently, π–π stacking has been identified as the interaction governing the adsorption of nucleobases on graphitic systems such as CNTs[18] and graphene.[19,20] The study of π–π stacking in adsorbate–graphene systems is also relevant for the use of graphene as a drug-delivery agent because the attachment of aromatic drug molecules to graphene is mainly through this type of noncovalent interaction.[21,22] In fact, in the interaction of aromatic hydrocarbons, aromatic amino acids and nucleobases with CNTs and graphene, another competing mode exists, in which the molecule adopts a perpendicular orientation with respect to the carbonaceous surface, which has been attributed to the presence of the so-called CH···π interaction.[23] This weak attraction between a C–H bond and a π system is a unique type of noncovalent interaction in which the π electrons can be viewed as the proton acceptor and play a significant role in aromatic π networks in proteins.[24] The other weak, but not negligible, interactions are NH···π interactions, which have been identified to exist between the amino groups of nucleobases and graphene.[25] Moreover, if substituted derivatives of benzene are adsorbed on graphene, other interactions compete with the π–π stacking, giving rise to nonplanar structures. The aromatic ring of benzoic and isophthalic acids show significant tilting with respect the graphene surface, with the carboxyl groups oriented to the graphene.[26] By contrast, L-leucine, a non-aromatic molecule, adopts a quasi-parallel geometrical configuration if it is adsorbed on graphene, maximizing the pairwise van der Waals attractions with the C atoms of graphene.[27] We note that this type of system shows a rich variety of interactions that make the analysis more complex in comparison with the adsorption of smaller molecules with CNTs and graphene.

The theoretical study of the adsorption of biological molecules on carbon nanosystems based on graphene sheets and graphene nanoribbons is a field of considerable interest because a great number of questions exist in experimental research regarding the detection of these molecules. Furthermore, determining the nature of the binding of these molecules is of fundamental importance considering the multiple contributions to their stabilization on carbonaceous surfaces. Taking this into account in the present work, the adsorption of a DA molecule on the surface of perfect graphene (DA–G system) was studied within the framework of density functional theory (DFT). To that end, several different geometrical configurations for adsorbed DA were considered. Moreover, the reactivity of defective graphene having carbon monovacancies (DA–GV system) was investigated and compared to that of the regular surface. Two theoretical approaches including dispersive forces allowed us to formulate a realistic description of these systems and to reveal the role of noncovalent interactions. The π–π interaction was carefully examined in terms of the electronic structure and the NCI. The formation of a hydrogen bond in the AB-stacked mode for DA–GV might be related to the coupling between the HOMO of DA and a GV vacancy state. Other properties such as the surface reconstruction and the electron charge transfer between adsorbate and substrate were also analyzed.

2. Results and Discussion

2.1. The DA–G System

In order to study the adsorption of DA molecules on perfect graphene, six configurations were considered, which are shown in Figures 1 a–f. In the AB stack (S-ab) and AA stack (S-aa) configurations the DA molecule is parallel to the graphene sheet, with the ethylamine group oriented toward the vacuum. In the case of the S-ab configuration, the ring of the DA molecule is centered over a carbon atom of a graphene ring below, as with AB stacking according to Bernal's nomenclature for graphene bilayers, whereas for the S-aa configuration, the AA stacking was considered.[28] In the down (D) configuration, the DA molecule is also parallel to the graphene sheet but with the ethylamine group oriented toward the surface of graphene; for this structure, AA stacking was considered. In the lateral (L) configuration, the ring plane of DA molecule is arranged perpendicularly to the graphene plane, whereas the axis passing through the hydroxy group of the DA ring and the ethylamine group in the *para*-position of this same ring is arranged in parallel to the graphene plane. However, in perpendicular configurations, this axis is oriented perpendicularly to the graphene plane. There are two perpendicular orientations, perpendicular ethylamine (P-ea) and perpendicular OH (P-oh). In the former case, the ethylamine group is oriented toward the surface of graphene, whereas in the P-oh structure, the hydroxy group has this orientation.

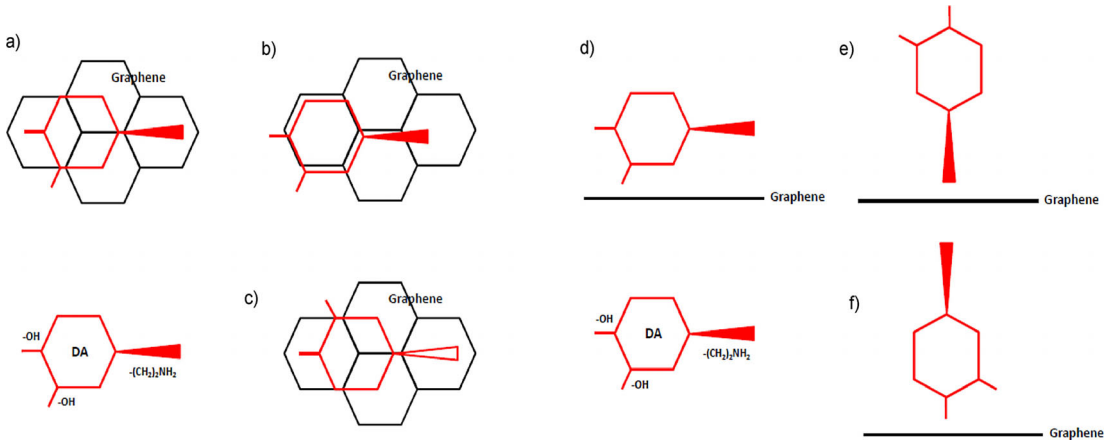

Figure 1. Geometrical configurations for a) S-ab, b) S-aa, c) D, d) L, e) P-ea and f) P-oh modes of DA adsorption on graphene.

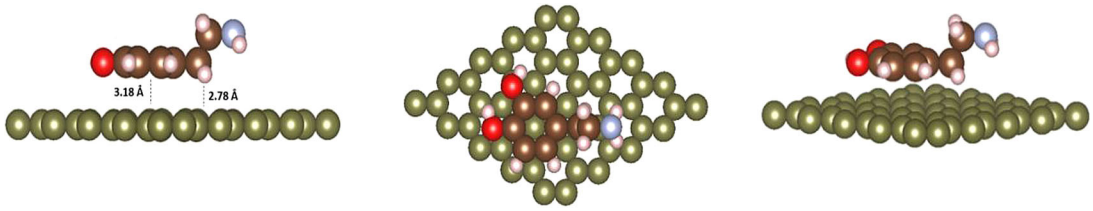

Figure 2. Optimized geometry for the DA–G system in the S-ab mode (DFT-D2 results). Lateral, top and perspective views. Graphene carbon atoms: green; DA carbon atoms: brown balls; oxygen: red; nitrogen: light blue; hydrogen: small white.

After the optimization of S-ab site was performed according to the DFT-D2 method, the DA molecule adopted a geometric configuration (Figure 2). The other sites are also depicted in Figures S1–S5 in the Supporting Information. The values of adsorption energy, calculated with both DFT-D2 and vdW-DF2 methods, are shown in Table 1, and those of the geometric parameters are summarized in Tables 2 and 3. As a reference, the interatomic distances calculated with the DFT-D2 method for the free DA molecule are indicated in Figure 3. In general, the S-ab and S-aa configurations remain almost parallel to the surface, whereas the P-ea and P-oh configurations are approximately perpendicular. In the D site, the plane of the DA molecule forms an angle of 13.98° with respect to the surface of graphene. Furthermore, in the L site, the axis passing through the ring groups in the *para*-position forms an angle of 20.95° with respect to the surface.

Firstly focusing on results calculated with DFT-D2, from Table 1 we can observe that S-ab, S-aa, and D sites are the most favored with E_{ads} values of approximately −0.70 eV, and the P-ea and P-oh site are the less favored, with about −0.20 eV. An intermediate situation is present for the L configuration, with approximately −0.60 eV. In particular, the S-ab site is more favorable than the S-aa site by nearly 0.05 eV. This type of configuration corresponds to the Bernal's AB stacking for two adjacent graphene sheets in graphite.[29] Therefore, the adsorption of DA on regular graphene shows behavior resem-

Table 1. Adsorption energy, E_{ads}, calculated with the DFT-D2 and vdW-DF2 methods and E_{GGA} and E_{vdW} components of E_{ads} (DFT-D2) for the DA–G system (in eV).

Energy	Site					
	S-ab	S-aa	D	L	P-ea	P-oh
E_{ads} (DFT-D2)	−0.74	−0.70	−0.69	−0.60	−0.25	−0.23
E_{GGA}	0.20	0.15	0.15	0.01	−0.04	−0.01
E_{vdW}	−0.94	−0.85	−0.84	−0.61	−0.21	−0.22
E_{ads} (vdW-DF2)	−0.70	−0.72	−0.71	−0.56	−0.20	−0.21

Table 2. Geometrical parameters [Å] for the DA–G system, calculated with the DFT-D2 method.

Geometrical parameter[a]	Site					
	S-ab	S-aa	D	L	P-ea	P-oh
d_{H1-C}	2.78	2.98	–	2.92	–	–
d_{H2-C}	2.85	2.75	–	–	–	–
d_{H3-C}	–	–	–	2.42	–	–
d_{H4-C}	–	–	–	2.70	2.85	–
d_{H5-C}	–	–	2.63	–	–	–
d_{H6-C}	–	–	2.80	–	–	–
d_{H7-C}	–	–	–	2.56	–	–
d_{H8-C}	–	–	–	–	2.96	–
d_{H9-C}	–	–	–	–	–	2.62
d_{O1-C}	–	–	3.11	–	–	2.98
d_{O2-H3}	0.97	0.98	0.98	0.98	0.97	0.97
h_{DA-G}	3.18	3.30	3.64	4.91	8.06	5.68
Δz_G	−0.07	−0.07	−0.03	−0.04	−0.01	−0.04

[a] d_{A-B}: Interatomic distance between atoms A and B; h_{DA-G}: distance between DA ring and graphene surface; Δz_G: graphene deformation. Atom designations are those used in Figure 3.

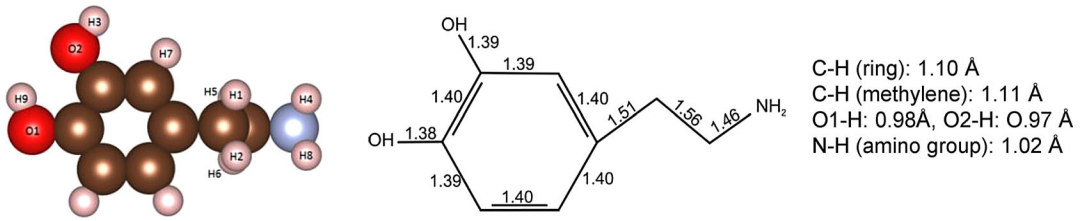

Figure 3. The main interatomic distances for a free DA molecule calculated with the DFT-D2 method. Atom colors are those used in Figure 3.

Table 3. Geometrical parameters [Å] for the DA–G system, calculated with the vdW-DF2 method.

Geometrical parameter[a]	Site					
	S-ab	S-aa	D	L	P-ea	P-oh
d_{H1-C}	2.89	3.12	–	3.05	–	–
d_{H2-C}	2.95	2.89	–	–	–	–
d_{H3-C}	–	–	–	2.5	–	–
d_{H4-C}	–	–	–	2.87	2.86	–
d_{H5-C}	–	–	2.75	–	–	–
d_{H6-C}	–	–	2.91	–	–	–
d_{H7-C}	–	–	–	2.65	–	–
d_{H8-C}	–	–	–	–	2.97	–
d_{H9-C}	–	–	–	–	–	2.63
d_{O1-C}	–	–	3.25	–	–	2.99
d_{O2-H3}	0.97	0.97	0.98	0.98	0.97	0.97
h_{DA-G}	3.39	3.38	3.77	5.02	8.07	5.69
Δz_G	−0.10	0.00	−0.08	−0.05	−0.02	−0.05

[a] d_{A-B}: Interatomic distance between atoms A and B; h_{DA-G}: distance between DA ring and graphene surface; Δz_G: graphene deformation. Atom designations are those used in Figure 3.

bling that of nucleobases, that is, the stacking configurations are favoring over the perpendicular or "T" configurations; the former being related to the presence of π–π interactions, the latter to CH···π interactions.[19,23] From the data in Table 2, Figure 2 and Figures S1–S5, we note that the minimum interatomic distances between DA and graphene correspond to the H–C distances (H atom from DA and C atom from graphene) in the range 2.63–2.78 Å for S-ab, S-aa and D sites, and in the range 2.42–2.85 Å for L, P-ea and P-oh sites. In the case of S-ab and S-aa sites, the hydrogen atom involved belongs to the first methylene of the ethylamine group, whereas in the case of the D site, to the second methylene of this group. At L and P-oh sites, the hydrogen atom involved can belong to either the DA hydroxy groups, whereas at the P-ea site, it belongs to the primary amino group.

The vertical distance between the center of DA ring and the graphene surface for the quasi-parallel configurations is in the range 3.18–3.30 Å. This interval is near to the reported distance between graphene sheets, 3.35 Å.[30]

Regarding the intramolecular interatomic distances in a DA molecule, we note that they are practically unchanged with respect to the free molecule (Figure 3), except for one C–H bond of the first methylene group and the O–H bond of the *meta*-hydroxy group for D and L sites, respectively (oriented toward the graphene surface), which are stretched by 0.01 Å. The average changes of the normal coordinate for C atoms nearest to DA, calculated with respect to the graphene plane, are reported in Table 2. We note that these C atoms at S-ab and S-aa sites undergo a negative relaxation of −0.07 Å with respect to the bare surface due to perturbation of DA molecule. For the other sites, this relaxation is of smaller magnitude, in the range −0.01 to −0.04 Å.

In Tables 1 and 3 the E_{ads} values and the geometric parameters obtained by using the vdW-DF2 method are shown, respectively. We could observe that E_{ads} values are similar to those calculated with the DFT-D2 method—the S-ab, L, P-ea and P-oh sites, are comparatively less stable, by 0.02–0.05 eV, and the S-aa and D sites, slightly more stable, by 0.01–0.02 eV. In particular, the AB-stacking geometry is slightly less stable than AA-stacking, by 0.02 eV, compared to the result obtained with DFT-D2. Regarding the minimum interatomic distances between DA and graphene, they are 0.11 to 0.14 Å longer for S-ab, S-aa and D sites than those calculated using the DFT-D2 method. Furthermore, this distance is 0.08 Å longer for the L site, and slightly longer, by 0.01 Å, for P-ea and P-oh sites. At D and L sites, tilts of 14.68° and 20.51° are produced, respectively. On the other hand, the vertical distance between the center of DA ring and the graphene surface turns out to be 0.08–0.21 Å longer for the S-ab, S-aa and D configurations. Recently, it was reported that the intermolecular distances between nucleobases and graphene are found to be in the following order: DFT-D2 < vdW-DF2.[19] This observation might also be related to the fact that if interatomic distances between molecules presenting dispersive interactions are calculated with vdW-DF2, they are up to 0.3–0.4 Å higher than those calculated using coupled-cluster methods with single, double and perturbative triple excitations [CCSD(T)].[31] However, from the previous comparison, it is clear that DFT-D2 provides an optimization near to that obtained with the more elaborate vdW-DF2 technique. The DFT-D2 method offers the possibility of evaluating the contribution of the dispersive interactions to the adsorption energy. This contribution is designated in Table 1 as E_{vdW} and the non-vdW contribution from the standard exchange and correlation interactions, is termed E_{GGA}. From the E_{VDW} and E_{GGA} values summarized in Table 1, we can observe that for S-ab, S-aa and D sites, the first contribution is in the range −0.84 to −0.94 eV, whereas the second contribution is in the range 0.15–0.20 eV. For L, P-ea and P-oh sites, the second contribution is almost negligible. It is notable that for the first three sites the electronic contribution is repulsive, a point that will be discussed later in this paper.

No experimental works related to the DA–G system using surface physics techniques have been previously published;

only results corresponding mostly to electrochemical methods can be found in the literature. In contrast, a recent DFT theoretical study for this system performed with a localized basis and periodic conditions has been reported.[32] In this latter work on a DA molecule adsorbed in a stacked geometrical mode, an adsorption energy of −0.18 eV and a distance between rings of approximately 2.84 Å were reported. The magnitude of this energy is smaller than those obtained here (0.52–0.54 eV), and the distance is 0.46 Å smaller than in our calculation. In an earlier DFT calculation about the adsorption of nucleobases on graphite based on a localized basis and a cluster model, adsorption energies in the range −0.52 to −0.76 eV are reported, with a distance between the nucleobase ring and graphene of 3.2–3.3 Å.[33] Furthermore, in a DFT-based study on an adenine–graphene system performed with a flat-wave basis and periodic conditions,[34] the calculated adsorption energy was approximately −0.95 eV and the distance between the adenine ring and graphene was almost 3.15 Å. In another theoretical study concerning the adsorption of nucleobases on graphene, based also on DFT and second-order Møller–Plesset perturbation theory (MP2) and implemented with a localized basis and a cluster model, adsorption energies in the range −0.74 to −1.07 eV were reported for a vertical distance between rings of 3.5 Å.[35] More recent calculations performed using the DFT-D2 method for the same system gave E_{ads} values in the range −0.52 to −0.77 eV with vertical distances between rings of 3.13–3.22 Å.[19]

In order to study possible charge transfer between adsorbate and substrate, the variation of the electronic charge density, $\Delta\rho$, of the DA–G system was calculated with respect to the isolated fragments constituted by the DA molecule and the graphene substrate. In Figure 4a the $\Delta\rho$ distribution corresponding to DA adsorbed on the S-ab site and calculated with the charge densities of the DFT-D2 method, provided by the generalized gradient approximation (GGA) functional, is shown. A significant redistribution of the electron charge density on both adsorbate and substrate can be observed, with an increase (Figure 4a, blue color) in certain regions and a decrease (Figure 4a, red color) in others.

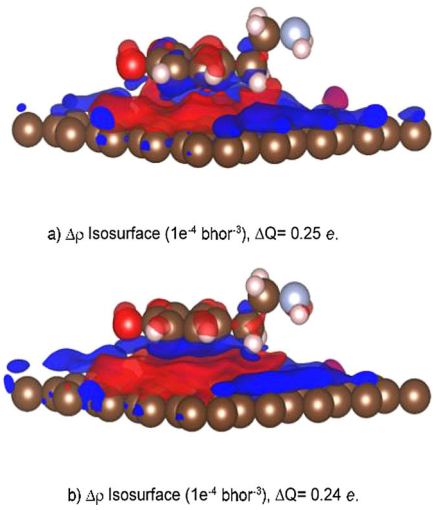

Figure 4. Charge density difference plots ($\Delta\rho$) and Voronoi atomic charge changes (ΔQ) for the DA–G system in the S-ab mode. a) DFT-D2 results and b) vdW-DF2 results. Positive values of $\Delta\rho$ are shown in red, negative values in blue. DA and graphene carbon atoms: brown; other atoms are as in Figure 3.

To quantify this effect, $\Delta\rho$ was integrated into polyhedrons centered on each atom *i*, the faces of which are defined by the planes of a Wigner–Seitz cell, following Voronoi's procedure.[36] Thus, in this way, we were able to calculate the electronic charge variation ΔQ_i around this atom. If we performed the summation of the ΔQ_i values corresponding to the DA molecule, the electronic charge variation of this molecule, ΔQ_{DA}, can be calculated. Table 4 summarizes the ΔQ_{DA} values for the different adsorption sites. The sum of ΔQ_i values for graphene is exactly the opposite of ΔQ_{DA}.

Table 4. Charge differences, ΔQ, and the corresponding adsorbate–substrate and total electrostatic energies, E_{Ea-s} and E_{Etot}, respectively, for the DA–G system.

	Method	Site					
		S-ab	S-aa	D	L	P-ea	P-oh
ΔQ [e]	DFT-D2	0.25	0.27	0.38	0.47	0.11	0.09
	vdW-DF2	0.24	0.20	0.29	0.40	0.12	0.09
E_{Ea-s} [eV]	DFT-D2	−0.20	−0.23	−0.45	−0.72	−0.05	−0.04
	vdW-DF2	−0.13	−0.06	−0.27	−0.52	−0.06	−0.04
E_{Etot} [eV]	DFT-D2	−0.38	0.04	0.07	0.07	0.01	0.00
	vdW-DF2	0.06	0.06	0.06	0.06	0.01	0.01

We note that the ΔQ_{DA} values are consistent with an electron transfer from graphene to DA. This transfer is about 0.3 e for S-ab and S-aa sites, 0.4–0.5 e for D and L sites, and 0.1 e for P-ea and P-oh sites. An important aspect to be emphasized, which is evident from Figure 4a, is that the charge distributions are delocalized in both adsorbate and substrate fragments. If we want to evaluate the energy of electrostatic origin, we must consider not only the electrostatic interaction between adsorbate and substrate, E_{Ea-s}, but also the contribution from the electrostatic interactions within each fragment. The values corresponding to E_{Ea-s} and the total electrostatic energy including such inner interactions, E_{Etot}, are shown in Table 4. These can be determined approximately from the obtained ΔQ_i values, by considering point charges centered on each atom. It is clear that this method of calculation only gives a rather crude approximation to the actual values of E_{Ea-s} and E_{Etot}, but it shows how the interactions of electrostatic origin behave qualitatively. It can be seen that at increasing values of ΔQ_{DA}, the amount of the attractive energy E_{Ea-s} between DA and graphene also grows. Conversely, the internal repulsion energies within the fragments counteract E_{Ea-s}, giving a small E_{Etot} value. Therefore, although charge transfer occurs between DA and graphene, the electrostatic energy is not a generally predominant factor in the stability of the DA–G system. An exception would be the case of the S-ab site, at which the permanent dipole of the DA induces charges of opposite sign on graphene that tend to attract each other, giving a negative E_{Etot} value with a higher magnitude than E_{Ea-s}. This can be at-

tributed, in the case of this configuration, to a favorable shielding response from the π electronic cloud in graphene if the DA axis is aligned along a C–C bond at the surface. Looking at Figure 4b and Table 4 we note that, if the charge densities provided by the vdW-DF2 method are used, we attain the same tendencies exhibited by DFT-D2 method. The electron charge transfer from graphene to DA is similar for S-ab, P-ea, and P-oh sites, and 15–25% lower for S-aa, D and L sites, whereas the magnitudes of the associated electrostatic energies are generally smaller.

With the aim of analyzing the electronic structure inherent to the DA–G system, we calculated the projected density of states (PDOS) on specific fragments. Although the results discussed here are those corresponding to the single-particle Kohn–Sham orbitals calculated with the GGA approximation used in DFT-D2, similar results were obtained with the exchange-correlation functional used in vdW-DF2. In Figure 5 the

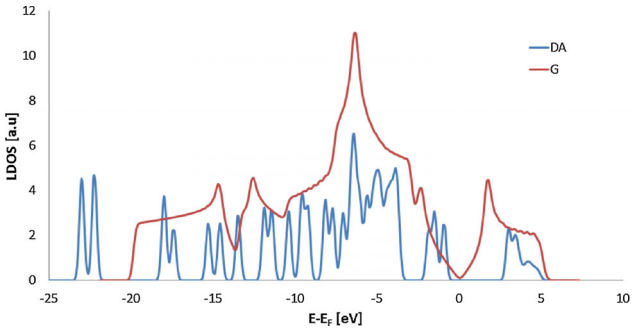

Figure 5. Electronic PDOS of the DA–G system calculated with the DFT-D2 method, for DA placed far from graphene.

PDOS on DA and graphene fragments, if they are far apart, are shown. The valence and conduction bands of graphene, with the Dirac point making the contact between these bands is also apparent, as are the HOMO and LUMO of DA below and above the Fermi level, respectively. The charge transfer discussed above can be explained using arguments based on the frontier orbitals of graphene and DA.[37]

Indeed, we note that, due to the coupling of the DA HOMO and the unoccupied graphene states above its Fermi level (Figure 6), electron donation to graphene is to be expected. However, the coupling of the DA LUMO and the occupied graphene states below its Fermi level implies a backdonation toward the DA. Taking into account this reasoning and the

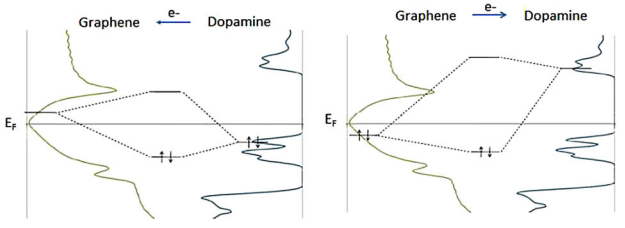

Figure 6. Frontier molecular orbital interactions for a DA molecule and a regular graphene sheet.

ΔQ_{DA} values as discussed, we expect that the coupling between the DA LUMO and the occupied graphene states predominates in the DA–G system.

Figure 7 shows a comparison between the projected PDOS corresponding to DA adsorbed on graphene at an S-ab site and that for DA placed far apart from graphene, that is, a situa-

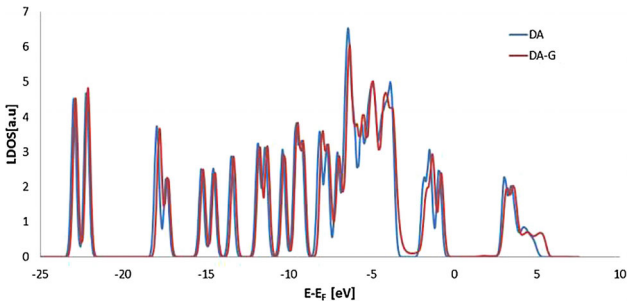

Figure 7. Electronic PDOS on the DA fragment for a DA molecule placed far from graphene (DA) and for the DA–G system in the S-ab mode (DA–G).

tion with no interaction between adsorbate and substrate. It can be observed that upon adsorption the bands between −8 and 7 eV undergo a small but non-negligible widening that reveals coupling between the DA orbitals and those of graphene; this is particularly true for states around −6 eV. In Figure 8, it is possible to identify, for the S-ab site, the projected PDOS on the DA ring, on its amino group and on the graphene carbon atoms near to DA. Considering the spatial arrangement of adsorbate and substrate in this adsorption mode, a favorable coupling is expected between the π orbitals of the DA ring and those of the graphene rings. The bonding and antibonding states resulting from one of these couplings are also shown schematically in Figure 8.

Notably, because both states are doubly occupied, a four-electron repulsive interaction is produced. The latter observation is in agreement with the results described above, indicating a repulsive interaction due to the non-van der Waals contribution E_{GGA}. This fact has also been shown in Ref. [35] for the interaction between adenine and graphene. At adsorbate–substrate distances of less than 3 Å, the kinetic energy contribution to the energy of single-particle Kohn–Sham orbitals is much more relevant than the attractive contribution due to electronic exchange and correlation effects. Conversely, the energy decomposition analysis performed on intermolecular interaction energies obtained with the B97-D functional (a hybrid GGA exchange-correlation functional with dispersion correction) for nucleobases adsorbed on graphene exhibited large repulsive interactions of electron exchange origin.[38]

As previously discussed, the dispersive interaction is essential for defining stable adsorption configurations for the DA–G system. In order to study this interaction in more depth, we performed an analysis using the noncovalent index (NCI). Recently, this index was used to characterize the dispersive interactions in the adsorption of $As(OH)_3$ on doped graphene.[39] Figure 9a shows the 2D NCI plot for DA–G in the S-ab adsorption mode, calculated with the charge density calculated with

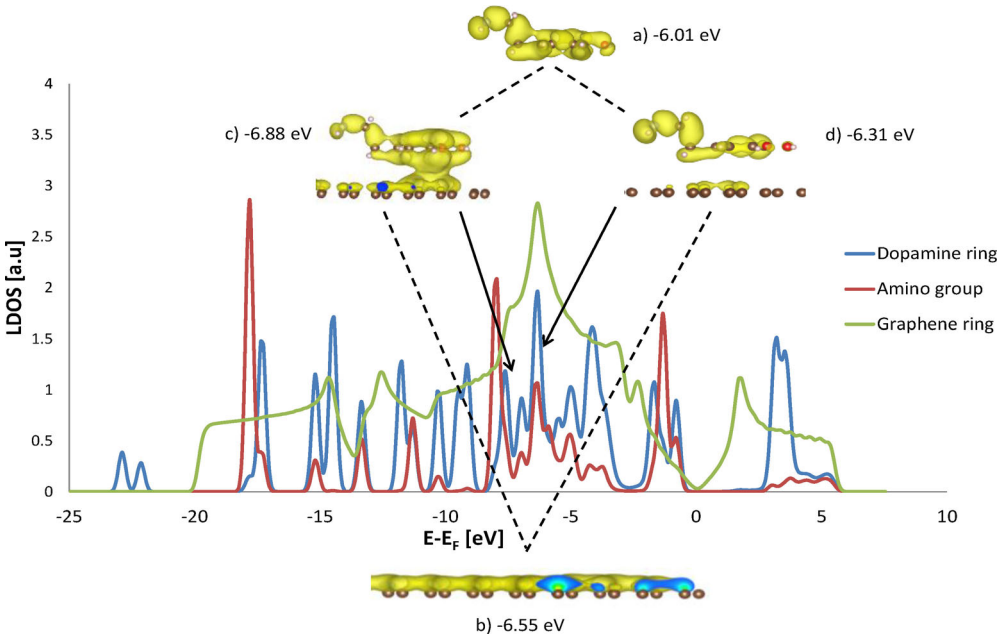

Figure 8. Electronic PDOS on the DA ring (dopamine ring), the DA amino group (amino group) and on graphene C atoms near to DA (graphene ring), for the DA–G system in the S-ab mode. The electronic charge density (ρ) isosurfaces (1 e^{-4} $bohr^{-3}$) of selected states for a) isolated DA and b) isolated graphene, and their c) bonding and d) antibonding combinations, are displayed. The corresponding energy eigenvalues are also indicated. The calculations of ρ were performed at the Γ point.

the DFT-D2 method. The appearance of a steep peak for negative and near zero values of sign $(\lambda_2)\rho$ is observed. This is an indication of the presence of dispersive interactions. In the same figure, the 3D plot for negative values of λ_2 shows an annular region (in green) located between the DA ring and its nearest graphene ring, associated with van der Waals interactions. The electronic charge density could be attributed to the electronic π clouds of these rings. Figure 9b shows the NCI plots calculated with the electron charge density derived from the vdW-DF2 method. The latter is obtained in a self-consistent way, including dispersive effects. It can be seen that these plots give the same qualitative results as those provided by the GGA charge density.

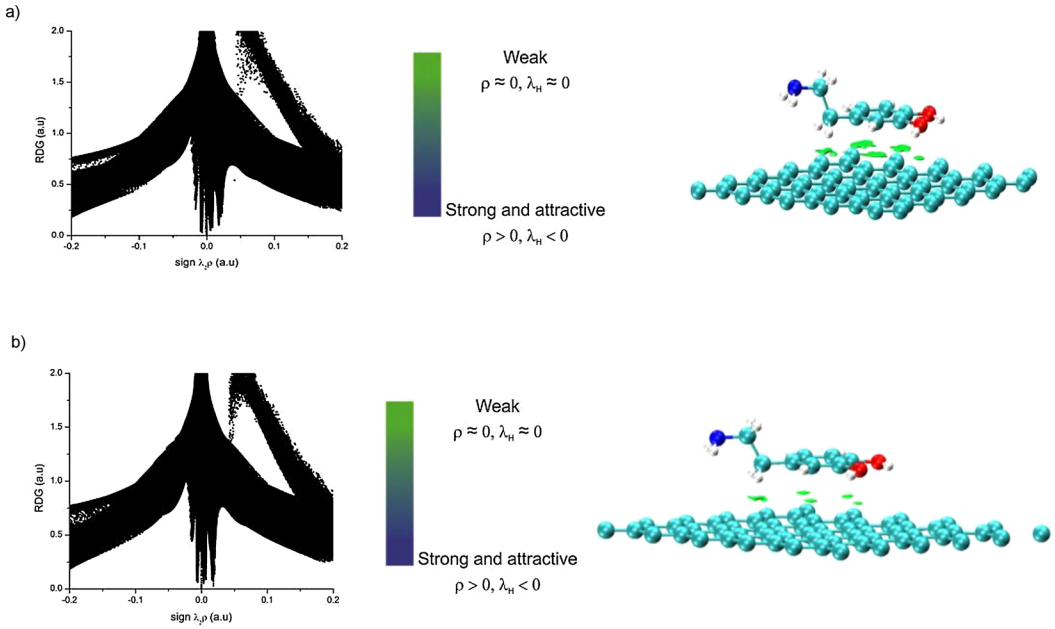

Figure 9. 2D (left panel) and 3D (right panel, perspective view) NCI plots for the DA–G system in the S-ab mode, calculated from the charge density from a) DFT-D2 and b) vdW-DF2 methods. 3D NCI isosurfaces correspond to $s = 0.25$ and a color scale of $-0.01 \leq \text{sign}(\lambda_2)\rho \leq 0$ $bohr^{-3}$.

2.2. The DA–GV System

In this section the results for DA adsorbed on graphene with monovacancies are discussed. Six adsorption modes were again considered, which are shown in Figures 10a–f. In the geometrical configurations designated S-ab, S-aa and D, the DA molecule is placed parallel to the defective graphene sheet, with the ethylamine group oriented toward the vacuum in the S-ab and S-aa configurations, and toward the surface of graphene in the case of the D configuration. Whereas at the S-ab site the ring of the DA adopts a configuration analogous to that of Bernal's AB stacking, in the S-aa and D sites, an in-plane rotated AA stacking was considered. The remaining configurations, L, P-ea, and P-oh, are similar to those described for the surface without vacancies.

Although no magnetism is present in perfect graphene, it arises if carbon vacancies are generated in the graphene lattice.[40] In the case of monovacancies, different values for the magnetization values have been reported, in the range 0.45–1.14 μ_B per vacancy.[40,41] Here, using our GV model for defective graphene, a value of 0.76 μ_B per vacancy was obtained. Hence, it is appropriate to make polarized spin calculations in the case of DA adsorption on GV. The evaluations performed with the DFT-D2 method indicate that the total energy results for the DA–GV system at the spin-polarized level are less favorable, in the range 0.01–0.35 eV, with respect to those obtained at the non-spin-polarized level, for a magnetization in the range 0.4–0.8 μ_B per vacancy. Therefore the DA–GV system must be treated as a closed-shell electronic system. Although the adsorption energy values are reported here with reference to the nonmagnetic GV surface, the E_{ads} values expressed with respect to the magnetic GV surface turn out to be only 0.07 eV less negative. It is worth underlining that if a monovacancy is produced, a Jahn–Teller distortion occurs and the trigonal symmetry of the regular graphene surface is lost.[40] The carbon atoms of lower coordination in the monovacancy are the vertices of an isosceles triangle composed by two long and one short sides; the longest side being 2.60 Å and the shortest, 2.31 Å, at the non-spin polarized level of calculation, and 2.60 and 2.20 Å, respectively, at the spin-polarized level.

After optimizing the S-ab site with the DFT-D2 method, the DA molecule adopted a geometric configuration, as shown in Figure 11. The other sites are depicted likewise in Figures S6–S10.

The values of adsorption energy, calculated with DFT-D2 as well as with vdW-DF2, are shown in Table 5, and those of the geometric parameters are summarized in Tables 6 and 7. Similarly to the sites described for the DA–G system, it can be observed that the S-ab and S-aa modes of adsorption are almost parallel to the surface, and the P-ea and P-oh modes remain nearly perpendicular. Similarly as for the DA–G system, at the D site the plane of DA molecule shows a non-negligible tilt (at an angle of 15.83° with respect to the GV surface), and in addition, at the L site the axis passing through the ring groups in the *para*-position is also tilted (forming an angle of 16.01° with respect to the GV surface).

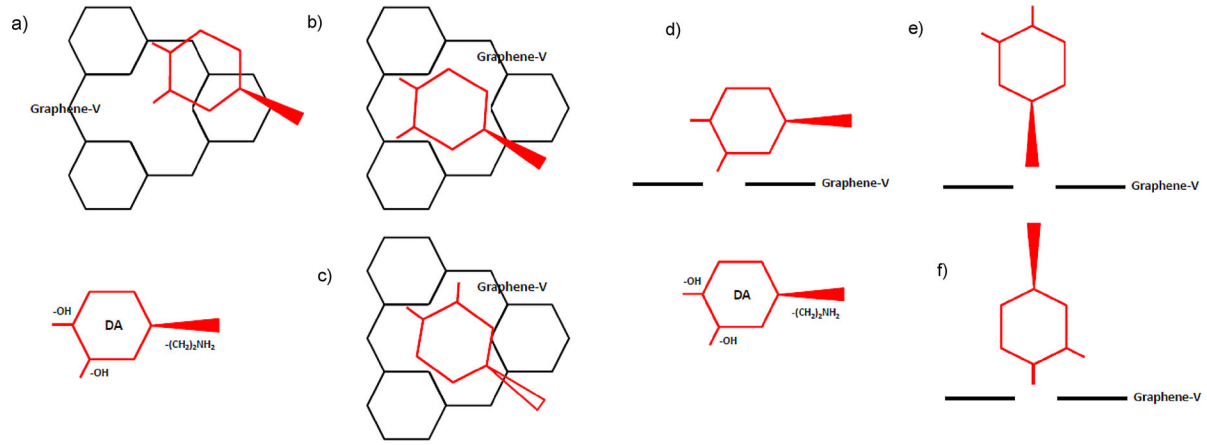

Figure 10. Geometrical configurations for a) S-ab, b) S-aa, c) D, d) L, e) P-ea and f) P-oh modes of DA adsorption on graphene with a monovacancy (graphene V).

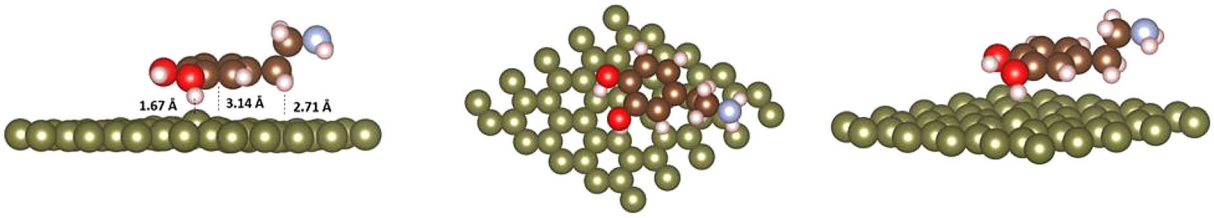

Figure 11. Optimized geometry for the DA–GV system in the S-ab mode (DFT-D2 results). Lateral, top and perspective views. Graphene carbon atoms: green; DA carbon atoms: brown; oxygen: red; nitrogen: light blue; hydrogen: white.

Table 5. Adsorption energy, E_{ads}, calculated with the DFT-D2 and vdW-DF2 methods and E_{GGA} and E_{vdW} components of E_{ads} (DFT-D2) for the DA–GV system (in eV).

Energy	Site					
	S-ab	S-aa	D	L	P-ea	P-oh
E_{ads} (DFT-D2)	−1.02	−0.65	−0.06	0.02	0.31	0.25
E_{GGA}	−0.13	0.18	0.68	0.69	0.55	0.55
E_{vdW}	−0.89	−0.83	−0.74	−0.67	−0.24	−0.30
E_{ads} (vdW-DF2)	−0.94	−0.67	−0.71	−0.59	−0.15	−0.30

Table 6. Geometrical parameters [Å] for the DA–GV system, calculated with the DFT-D2 method.

Geometrical parameter[a]	Site					
	S-ab	S-aa	D	L	P-ea	P-oh
d_{H1-C}	2.71	2.73	–	2.84	–	–
d_{H2-C}	2.95	2.78	–	–	–	–
d_{H3-C}	1.67	3.09	2.83	2.20	–	–
d_{H4-C}	–	–	–	2.61	2.59	–
d_{H5-C}	–	–	2.77	–	–	–
d_{H6-C}	–	–	2.95	–	–	–
d_{H7-C}	–	–	–	2.36	–	–
d_{H8-C}	–	–	–	–	2.86	–
d_{H9-C}	–	–	–	–	–	2.40
d_{O1-C}	–	–	–	–	–	3.00
d_{O2-C}	–	–	3.23	-	–	–
d_{O2-H3}	1.05	0.97	0.97	0.98	0.97	0.97
C–C′[b]	2.65	2.34	2.04	2.61	2.60	2.15
C′–C″[b]	2.25	2.60	2.58	2.12	2.12	2.63
C–C″[b]	2.65	2.59	2.59	2.63	2.61	2.64
h_{DA-G}	3.14	3.26	3.73	4.71	7.77	5.27
Δz_C	0.53	−0.39	−0.44	−0.60	−0.51	−0.60
Δz_G	0.01	−0.07	−0.01	−0.15	−0.11	−0.08

[a] d_{A-B}: Interatomic distance between atoms A and B; h_{DA-G}: distance between DA ring and graphene surface; Δz_C: maximum displacement of graphene carbon atom; Δz_G: graphene deformation. Atom designations are those used in Figure 3. [b] Naked GV surface: C–C′ (2.61 Å), C′–C″ (2.31 Å), C–C″ (2.60 Å).

Table 7. Geometrical parameters [Å] for the DA–GV system, calculated with the vdW-DF2 method.

Geometrical parameter[a]	Site					
	S-ab	S-aa	D	L	P-ea	P-oh
d_{H1-C}	2.80	2.92	–	3.29	–	–
d_{H2-C}	3.04	2.97	–	–	–	–
d_{H3-C}	1.86	3.36	2.94	2.37	–	–
d_{H4-C}	–	–	–	2.87	2.60	–
d_{H5-C}	–	–	2.85	–	–	–
d_{H6-C}	–	–	2.95	–	–	–
d_{H7-C}	–	–	–	3.23	–	–
d_{H8-C}	–	–	–	–	2.88	–
d_{H9-C}	–	–	–	–	–	2.44
d_{O1-C}	–	–	–	–	–	3.01
d_{O2-C}	–	–	3.33	–	–	–
d_{O2-H3}	1.01	0.97	0.97	0.98	0.97	0.97
C–C′[b]	2.68	2.37	2.37	2.60	2.65	2.36
C′–C″[b]	2.36	2.62	2.63	2.66	2.36	2.67
C–C″[b]	2.67	2.65	2.65	2.38	2.61	2.67
h_{DA-G}	3.30	3.48	3.78	5.10	7.77	5.27
Δz_C	0.56	−0.52	−0.49	−0.52	−0.52	−0.59
Δz_G	−0.01	−0.14	−0.09	−0.21	−0.11	−0.06

[a] d_{A-B}: Interatomic distance between atoms A and B; h_{DA-G}: distance between DA ring and graphene surface; Δz_C: maximum displacement of graphene carbon atom; Δz_G: graphene deformation. Atom designations are those used in Figure 3. [b] Naked GV surface: C–C′ (2.66 Å), C′–C″ (2.37 Å), C–C″ (2.63 Å).

Regarding in first place the results calculated with DFT-D2, from Table 5 it can be deduced that the S-ab and S-aa geometries are the most favored with Eads values in the range of −0.65 eV to −1.02 eV, in comparison with the D, with only −0.06 eV. The DA molecule is not stable on the L, P-ea and P-oh sites, where the adsorption is endothermic. The most favorable site is the S-ab, with an E_{ads} value of greater magnitude by 0.28 eV than that for the S-ab site on the perfect surface. Therefore, this site is the most exothermic of both perfect graphene and graphene with monovacancies. Moreover, from Table 6, Figure 11 and Figures S6–S10 it can be inferred that the minimum interatomic distances between DA and graphene correspond to the H–C distances (H atom from DA and C atom from GV). The shortest H–C distance is that of the S-ab site, 1.67 Å, being in the range 2.73–2.77 Å for S-aa and D sites, and in the range 2.20–2.59 Å for L, P-ea and P-oh sites. In the case of S-ab, L, and P-oh sites, the hydrogen atom involved belongs to a hydroxy group, whereas for S-aa and D sites, it is part of the first and second methylene groups, respectively. In the case of the P-ea site, the hydrogen atom of DA involved is part of the primary amino group. The vertical distance between the center of the DA ring and the graphene surface for the quasi-parallel configurations is in the range 3.14–3.26 Å, which is shifted by approximately 0.04 Å to smaller values with respect to perfect graphene. This result is in agreement with the E_{ads} values, which are greater in magnitude. In the case of the S-ab site, it should be noted that the hydroxy group in the *meta*-position is oriented toward one of the C atoms of lower coordination in the monovacancy, rising above the plane of graphene. Accordingly, a hydrogen bond between DA and the monovacancy, OH···C, is formed. The O–H bond relaxes from its length of 0.97 Å for the free molecule to 1.05 Å. The values of H–C distance, 1.67 Å, and O–H–C bond angle, 168.4°, are consistent with a hydrogen bond of intermediate strength.[42] Moreover, the length of the C–O bond, which is a neighbor to the *meta*-OH group, is shortened by 0.02 Å, whereas the ring C–C bond between the two hydroxy groups is stretched by 0.01 Å. In relation to the other intramolecular bond lengths of adsorbed DA, we can observe that, in general, they are similar to those of the free molecule, with the exception of the O–H bond of the *meta*-hydroxy group in the L adsorption mode, which is directed toward graphene and is stretched by 0.01 Å.

From the geometries shown in Figure 11 and Figures S6–S10, it is evident that one of the carbon atoms of the monovacancy suffers a normal displacement from the plane of graphene that is more significant than for others. Table 6 reports the change of the normal coordinate for this atom. Note that it is positive for the S-ab site, 0.53 Å, and negative for other sites, between −0.39 and −0.60 Å. If a mean of the normal coordinates for C atoms nearest to DA is taken (see Table 6), we

conclude that whereas the mean value for the S-ab site is very small and positive, it is still remarkably negative for the other sites. The carbon atoms of lower coordination in the monovacancy form the vertices of an isosceles triangle composed by two long and one short sides, having a longest side of 2.58–2.65 Å, and the shortest, of 2.04 to 2.15 Å (see Table 6). Therefore, the adsorption of DA on GV preserves the Jahn–Teller distortion mentioned above, contrary to the adsorption of Al atoms, upon which the trigonal symmetry is restored.[40] The vertex corresponding to the smallest angle of the isosceles triangle is the atom of the monovacancy that suffers the largest normal displacement. It is notable that for the S-ab site the C–C–C bond angle centered on this atom deviates by only −0.1° with respect to the 120° of sp^2 hybridization in perfect graphene, whereas for the other sites the deviation is larger, in the range 1.6–1.9°.

The results obtained using the vdW-DF2 method are summarized in Tables 5 and 7. We observed that the adsorption energy values for the S-ab and S-aa sites are similar to those calculated with the DFT-D2 method; in particular, the value for the S-ab site is nearly 0.1 eV more stable. The other sites have more negative E_{ads} values, by approximately −0.5 to −0.6 eV, if calculated with the vdW-DF2 method. Thus, at this level of calculation, all adsorption sites correspond to exothermic processes. Hence, the adsorption of DA on graphene with monovacancies studied by means of the vdW-DF2 method shows behavior resembling that of nucleobases, that is, favoring the stacking configurations versus the perpendicular or "T" configurations. This behavior is different to that obtained using the DFT-D2 method, in which the D site is much less favored than the S-ab and S-aa sites and the L site does not exhibit an intermediate binding strength. At D and L sites, tiltings of 15.63° and 19.37° are produced, respectively. The minimum interatomic distance between DA and GV, is 0.17–0.19 Å greater for the S-ab, S-aa and L sites than that calculated with the DFT-D2 method. For the D site, it is 0.08 Å greater, whereas for P-ea and P-oh sites, slightly greater (by 0.01–0.04 Å). Furthermore, the vertical distance between the center of the DA ring and the graphene surface for the quasi-parallel configurations is 0.16–0.22 Å greater. In other words, the geometrical results of vdW-DF2 method for DA–GV, compared those of DFT-D2, follow the same trend as the calculations for DA–G. Moreover, as a consequence of DA adsorption, the monovacancy carbon atoms undergo normal displacements similar to those calculated with the DFT-D2 method (Tables 6 and 7).

By inspecting the E_{ads} values reported in Table 5 calculated with the DFT-D2 method, it can be concluded that for S-ab, S-aa, D, and L sites, the E_{vdW} contribution is predominant (in the range −0.67 to −0.89 eV) compared to the E_{GGA} contribution, whereas for P-ea and P-oh sites it is of lower relevance (in the range −0.24 to −0.30 eV). The E_{GGA} contribution was found to be negative for the S-ab site (−0.13 eV) and positive for all other sites, and was particularly large for D, L, P-ea and P-oh modes of adsorption (in the range 0.55–0.69 eV). A comparison of the same type of site in DA–GV and DA–G systems reveals that although the E_{vdW} contribution is similar for both systems, the E_{GGA} contribution establishes the difference between these systems. In fact, the negative contribution for the S-ab site in DA–GV makes this adsorption mode the most stable, and is related to the formation of the hydrogen bond, whereas the highly repulsive value for D, L, P-ea and P-oh sites produces a great destabilization of these adsorption modes. Note that the adsorption energies for P-ea and P-oh sites in the DA–GV system calculated with the vdW-DF2 method are negative, whereas they are positive with the DFT-D2 method. This different behavior can be attributed to the different treatment of each functional with the local exchange and correlation effects.

Recently, the E_{ads} values for the DA molecule adsorbed in a stacked mode on graphene with monovacancies has been computed, giving a value of −0.11 eV.[32] This result is of much smaller magnitude, by 0.83–0.91 eV (S-ab site) and by 0.54–0.56 eV (S-aa site), than those obtained here. Furthermore, the reported distance between adsorbate and substrate rings is nearly 2.95 Å, that is, about 0.19–0.53 Å smaller in comparison with our calculations. Notably, and in contrast to our results, the DA–GV system was reported to be less favorable than the DA–G one.

The variation of the electronic charge density of the DA–GV system in the S-ab site, calculated with the DFT-D2 charge densities, is shown in Figure 12a. A significant redistribution of the electron charge density on both adsorbate and substrate can be observed, similarly to what occurs in DA–G. The values of ΔQ_{DA} obtained for the various adsorption sites of DA–GV are summarized in Table 8. We note that they are consistent with electron transfer from the substrate to the adsorbate. This transfer is greater than that calculated for the DA–G sites of similar designation (Table 4), by 0.35 e for the S-ab site, and 0.07 to 0.13 e for L, P-ea and P-oh sites. For the S-aa site the magnitudes are more similar, only 0.02 e smaller, and for the D site, 0.1 e smaller. According to the values of electrostatic energies E_{Ea-s} and E_{Etot} (Table 8), we observed that in general the latter are smaller in magnitude than the former, except for S-aa and L sites. In these adsorption modes the electrostatic repulsions within the fragments are relatively important, indicating that the charges would be less delocalized. The S-ab site exhibits the largest negative values of E_{Ea-s} and E_{Etot}, even than those calculated for the DA–G system, in agreement with the largest obtained value of ΔQ_{DA}. This specific polarization might explain, at least in part, the negative value of the E_{GGA} contribution to E_{ads} for this site, owing to the greater E_{Etot}. Figure 12b

Table 8. Charge differences, ΔQ, and the corresponding adsorbate–substrate and total electrostatic energies, E_{Ea-s} and E_{Etot}, respectively, for the DA–G system.

	Method	Site					
		S-ab	S-aa	D	L	P-ea	P-oh
ΔQ [e]	DFT-D2	0.60	0.25	0.29	0.54	0.18	0.22
	vdW-DF2	0.51	0.20	0.27	0.41	0.18	0.23
E_{Ea-s} [eV]	DFT-D2	−1.13	−0.08	−0.24	−0.25	−0.09	−0.14
	vdW-DF2	−0.70	−0.03	−0.18	−0.17	−0.09	−0.14
E_{Etot} [eV]	DFT-D2	−0.26	0.13	0.05	0.73	0.04	0.02
	vdW-DF2	−0.03	0.14	0.06	0.36	0.04	0.02

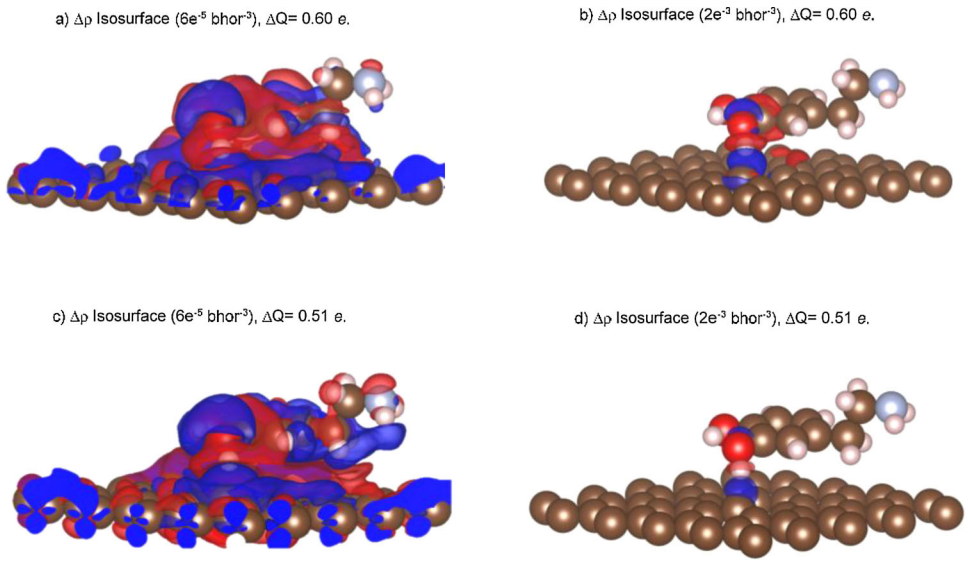

Figure 12. Charge density difference plots ($\Delta\rho$) and Voronoi atomic charge changes (ΔQ) for the DA–GV system in the S-ab mode. a) and b) DFT-D2 results; c) and d) vdW-DF2 results. Positive values of $\Delta\rho$ are shown in red, negative values in blue. DA and graphene carbon atoms: brown; the other atoms are shown as in Figure 11.

shows the $\Delta\rho$ isosurface corresponding to the S-ab site in the DA–GV system calculated for a greater $|\Delta\rho|$ than that shown in Figure 12a. Note the particular accumulation of electronic charge in the line between the H atom of the DA hydroxy group and the C atom of graphene that defines the OH···C bond mentioned above. This observation will be considered again later. From Figure 12c and d and Table 8, it can be seen that the charge densities provided by the vdW-DF2 method give trends analogous with those obtained with the DFT-D2 method. Specifically, the electron transfer from GV to DA is similar for S-aa, D, P-ea and P-oh sites and 15–25% lower for S-ab and L sites, whereas the magnitude of the associated electrostatic energies is equal or smaller.

Figure 13 shows the PDOS corresponding to DA and GV fragments if they are far apart, calculated with the GGA approximation used in DFT-D2 method. Similar results were obtained using vdW-D2. We see in the PDOS on graphene with monovacancies the presence of a peak located at the Fermi level that yields the disappearance of the Dirac point and

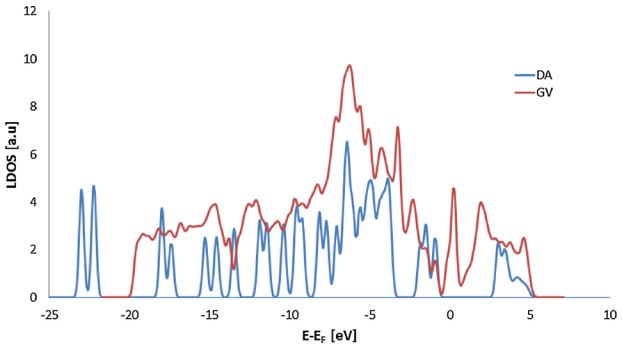

Figure 13. Electronic PDOS of the DA–GV system calculated with the DFT-D2 method, for DA placed far from graphene.

gives metallic character to the graphene. This peak is symmetrical with nearly equal contributions above and below the Fermi level. Another peak also arises at 0.35 eV below the Fermi level. The profile of the remaining states below and above the Fermi level maintains a similar shape to that of regular graphene. Therefore, if considering the possible couplings between the frontier levels of DA and GV it is of vital importance to take into account the contribution from the graphene states located below the Fermi level. Following the previously discussed analysis associated with Figure 6, we could infer that the backdonation of electronic charge to the DA molecule should be expected to be more significant than the donation to graphene. This is in agreement with the results of Tables 4 and 8, indicating that the charge transfer from graphene to DA is three times higher for DA adsorbed on graphene with monovacancies than on perfect graphene. It is pertinent to mention that the PDOS curves obtained for GV obtained at the non-spin-polarized level exhibit similar profiles for both spin projections in comparison with the PDOS at the spin-polarized level. In particular, the peak arising below the Fermi level corresponds to the majority spin contribution, as was shown in a previous study.[43]

In Figure 14 the projected PDOS corresponding to DA adsorbed on graphene with monovacancies at S-ab site is compared with that of DA far apart from graphene. We note that, as in the case of DA–G system, the bands between −8 and 7 eV undergo a small but not negligible widening. This can be related, as before, to a coupling between the π orbitals of the DA ring and those of GV, giving rise to the appearance of bonding and antibonding states and a four-electron repulsive interaction. In addition, the position of DA states with respect to GV states and its Fermi level shifts towards lower binding energies, by nearly 0.9 eV compared to the situation for far-distant fragments. This effect can be ascribed to the electron

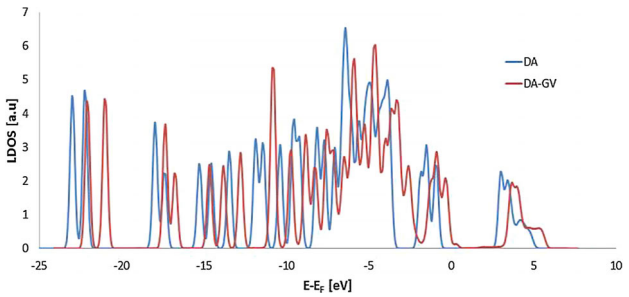

Figure 14. Electronic PDOS on the DA fragment for a DA molecule placed far from graphene with monovacancies (DA) and for the DA–GV system in the S-ab mode (DA-GV).

transfer between adsorbate and substrate, which destabilizes the levels of DA and stabilizes those of graphene. A similar observation has been outlined for the LUMO position of benzoic acids adsorbed on graphene, with respect to the Fermi level, as the degree of charge transfer from substrate to adsorbate increases.[22]

The PDOS for DA–GV in the S-ab mode of adsorption is shown in Figure 15. It is possible to identify the PDOS on the C atoms of DA ring, on its amino group and on those C atoms of GV nearest to DA (those that constitute the vacancy). Note the

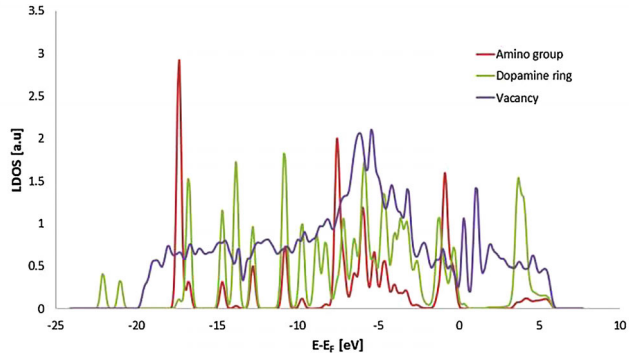

Figure 15. Electronic PDOS on the DA ring (dopamine ring), on the DA amino group (amino group) and on graphene C atoms near to the DA (vacancy), for the DA–GV system in the S-ab mode.

resemblance of PDOS profiles for the occupied states below −1 eV and the unoccupied states above 4 eV, corresponding to both the DA ring and the vacancy, to those calculated for the DA–G system. The same observation can be outlined for the PDOS corresponding to the DA amino group. The projected PDOS on the DA hydroxy group oriented toward the graphene surface and the projected PDOS on the less coordinated C atoms in the vacancy can be seen in Figure 16. We note the presence of a state located at −0.99 eV showing an electron density accumulation of covalent nature in the region between the H atom of the *meta*-hydroxy group of DA and one of the less-coordinated C atoms of the monovacancy. This state can be associated with the bonding combination between an occupied state of the isolated GV vacancy and the HOMO of free DA. Although this orbital becomes occupied, the antibonding counterpart, being above the Fermi level, is unoccupied. Stabilization of a covalent nature is produced owing to this coupling between states of DA and the GV vacancy. This state constitutes a covalent contribution to the OH···C hydrogen bond, as previously mentioned.

The hydrogen bonding, which tends to be much stronger than other noncovalent interactions on a per-atom basis, such as those arising from van der Waals forces, merits a careful description from the molecular orbital point of view.[44] This type of chemical bonding can be analyzed based on the electronic density, for example, by NCI analysis. Figure 17a shows the 2D NCI plot for DA–GV in the S-ab adsorption mode, calculated with the charge density derived using the DFT-D2 method.

We observe the appearance of two steep peaks for negative values of sign$(\lambda_2)\rho$, one close to zero and another at approximately −0.05. The first corresponds to the presence of dispersive interactions and the second to that of hydrogen bonding. The 3D plot for negative values of λ_2 is also shown in Figure 17a, showing an annular region (green) located between the DA ring and the nearest ring of graphene, associated with van der Waals interactions. Furthermore, a region appears between the H atom of DA hydroxy group oriented to one of the less-coordinated C atoms in the vacancy (blue). The sign$(\lambda_2)\rho$ value for this region indicates that it can be associated with an OH···C hydrogen bond.[45] This result confirms our previous proposal for the formation of a hydrogen bond in the S-ab mode of DA–GV. Figure 17b shows the NCI plots calculated with the electron charge density derived using the vdW-DF2 method. They give the same qualitative results as those obtained using the GGA electron charge density.

In the case of larger defects, such as divacancies that expose more unsaturated carbons, it is expected that the probability for the formation of a new hydrogen bond would increase, for example, that formed between the second hydroxy group of DA and one vacancy carbon. However, the increase in the number of vacancies does not correlate with greater adsorbate–substrate binding in other systems. For example, Pt clusters anchored at a divacancy can show a larger or a smaller binding energy than those anchored at a monovacancy depending on whether first principles or semiempirical methods are used.[46]

One important aspect of the DA–G and DA–GV systems is that DA is typically present in an aqueous environment. In this situation, the interaction of DA with water molecules might alter the DA–G and DA–GV binding modes above described. In order to quantify this solvent effect, the stability of the DA molecule in water as the dielectric medium in comparison with vacuum was evaluated by performing DFT calculations with a Gaussian basis set. The corresponding total energy values for a frozen geometry indicate that the DA molecule is approximately 0.3 eV more stable in an aqueous environment. Therefore, it can be expected that water–DA interactions compete with DA–G and DA–GV binding. Although this energy stabilization is approximately 30–50% the magnitude of the adsorption energy for the most favored sites, it does not change the general adsorption trends mentioned above for DA on graphene or on GV. On the other hand, we mention that our cal-

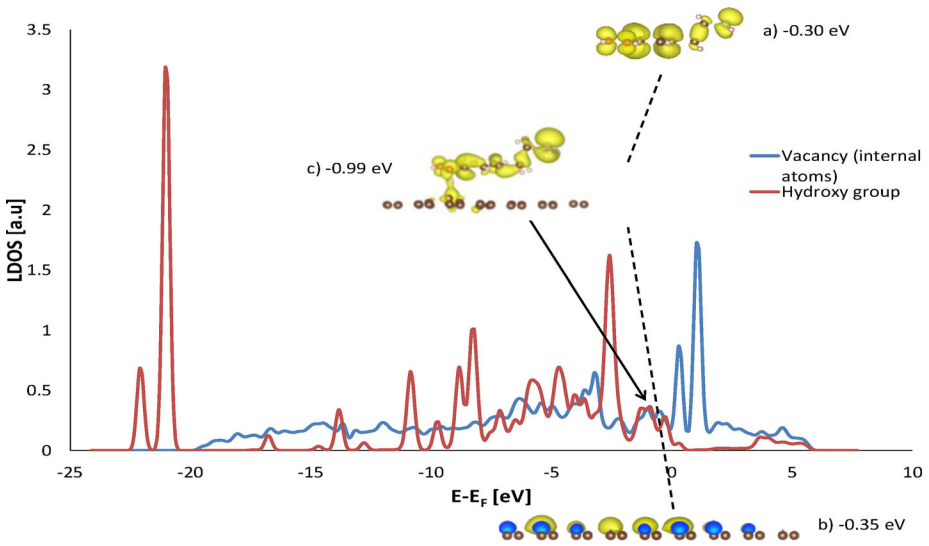

Figure 16. Electronic PDOS on the DA hydroxy group and on less-coordinated C atoms in the vacancy. The electronic charge density (ρ) isosurfaces (1 e$-^4$ bohr^{-3}) of selected states for a) isolated DA and b) isolated graphene, and their bonding combination (c), are displayed. The corresponding energy eigenvalues are also indicated. The calculations of ρ were performed at the Γ point.

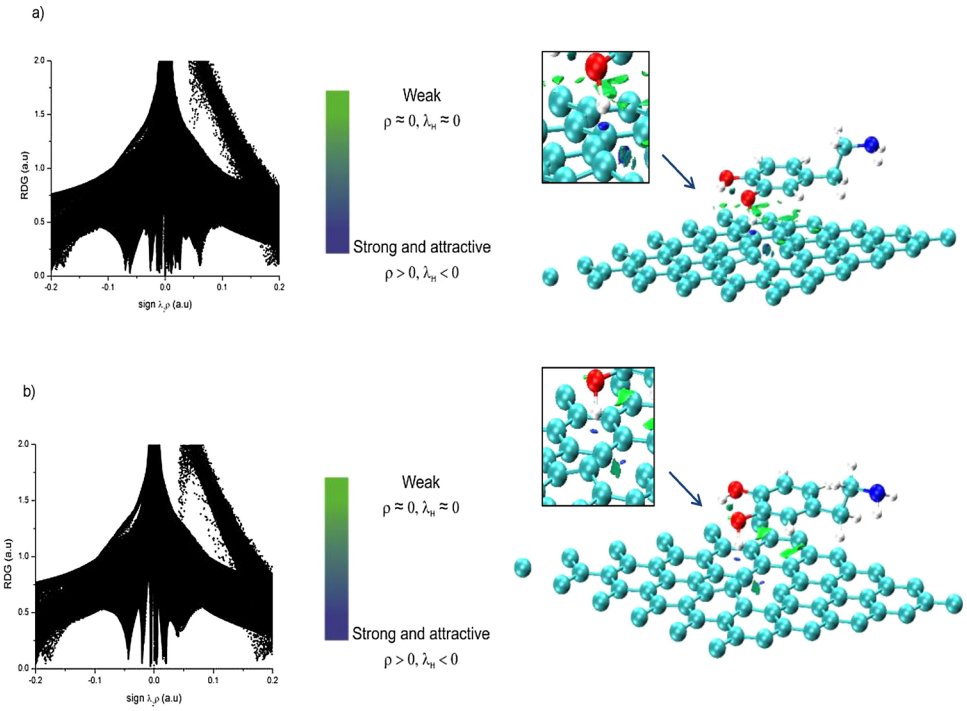

Figure 17. 2D (left panel) and 3D (right panel, perspective view) NCI plots for the DA–GV system in the S-ab mode, calculated from the charge density of a) DFT-D2, and b) vdW-DF2 methods. 3D NCI isosurfaces correspond to $s = 0.25$ and a color scale of $-0.01 \leq \text{sign}(\lambda_2)\rho \leq 0$ bohr^{-3}. Inset: Expanded region of hydrogen-bonding character.

culations do not consider thermal effects. If we take into account that the DA molecule has a kinetic energy of k_BT, this contribution is approximately 0.03 eV at 300 K, which would not change the results obtained in this study.

3. Conclusions

The bonding and geometry of DA–G and DA–GV systems were studied by using DFT-D2 and vdW-DF2 methods. On perfect graphene, two adsorption modes were identified, S-ab and S-aa, showing DA in a stacked configuration with the DA aromatic plane being almost parallel to the graphene sheet, two modes showing a somewhat significant degree of tilting, D

and L, and another two in which DA is oriented normally to the graphene sheet, P-ea and P-oh. The order of stability of these modes is S-ab ≫ S-aa ≫ D ≈ L ≫ P-ea ≈ P-oh for the DFT-D2 results and D ≈ S-ab ≈ S-aa > L ≫ P-o ≈ P-ea for vdW-DF2. A non-negligible electron transfer from graphene to the DA molecule takes place upon adsorption because the coupling between the LUMO of DA and occupied graphene states of the band are below the Dirac point. The contingent attractive electrostatic interaction is reduced due to the electrostatic repulsion within the fragments, with the result that the only significant attractive interaction comes from the dispersive forces. The latter must compete with a significant Pauli repulsion between the occupied π orbitals of the DA ring and those of graphene, giving adsorption energy values and inter-fragment distances of approximately 0.70 eV and 3.2 Å, respectively, for the most favored site. Despite the geometries being similar using both theoretical methods, the distances are approximately 0.2 Å greater for the vdW-DF2 method. NCI analysis confirmed the presence of an annular region of electron charge density located between the adsorbate and substrate aromatic rings related to van der Waals interactions. This result is evident using the electron charge density obtained with the GGA functional of DFT-D2, and was confirmed by using that obtained with the exchange-correlation functional of the vdW-DF2 method.

On defective graphene, six adsorption modes have been also identified, with the aromatic planes of DA and graphene either parallel or perpendicularly arranged with respect to the substrate. The stability ordering of the modes is S-ab > S-aa ≈ D > L ≫ P-oh > P-ea for DFT-D2 calculations and S-ab > D > S-aa > L ≫ P-ea > P-oh for vdW-DF2. In particular, the D and L modes are largely disfavored by the DFT-D2 method, in contrast to vdW-DF2. In all these modes of adsorption, magnetic states are disfavored and the monovacancy shows no trigonal symmetry. An electron transfer from graphene to the DA molecule occurs to a larger degree compared with regular graphene. In the S-ab configuration of adsorption, an OH···C hydrogen bond is formed, comprising the *meta*-hydroxy group of DA and one of the C atoms of lower coordination in the monovacancy. Stabilization of a covalent nature is also produced, associated with the bonding combination of an occupied state of the isolated GV vacancy and the HOMO of free DA and is accompanied by an accumulation of electronic charge in a line joining the H atom of the hydroxy group and the C atom of the GV vacancy. This hydrogen bond renders S-ab the most stable site, with an adsorption energy of approximately 0.4 eV greater magnitude than that of the S-aa site and about 0.3 eV larger than that for the S-ab site of perfect graphene. NCI analysis indicates the presence of an annular region of electronic charge related to van der Waals interactions and a region of hydrogen-bonding character between the DA hydroxy group and the GV vacancy. The inter-fragment distances for this site are approximately 0.3 Å larger for the vdW-DF2 method.

Another important conclusion is that on both graphene and GV surfaces the DA hydroxy groups in the two stacking modes and the D mode do not exhibit bending upwards or downwards from the DA ring plane, whereas in the L mode, one hydroxy group points outside the graphene sheet. Therefore, it could be argued that the L adsorption mode would favor the chemical attack of oxidizing agents on the DA molecule. Nevertheless, as the latter mode is at least 0.3 eV less favorable than the others, this type of reaction is feasible only with DA adsorbed parallel to graphene or in a D configuration.

Computational Details

The results reported in this work are based on the DFT formalism and were implemented by means of the Vienna Ab initio Simulation Program (VASP).[47,48] In this code, the Kohn–Sham equations are solved using a plane–wave basis and periodic boundary conditions. The electron–ion interactions are taken into account by the projector-augmented wave (PAW) potentials. The PAW method is a frozen-core all-electron method that uses the exact shape of the valence wavefunctions instead of pseudo-wavefunctions.[49,50] The fixed convergence of the plane–wave expansion was obtained with a cut-off energy of 400 eV. The perfect graphene sheet was modeled with a slab on which a hexagonal array of carbon atoms is replicated in the normal direction with a vacuum gap of 25 Å, thus minimizing the interaction between successive sheets. The graphene 2D array had a 5×5 supercell with 50 carbon atoms. The graphene sheet with a monovacancy was modeled by eliminating one carbon atom of this 5×5 supercell and relaxing the remaining carbon atoms. Integrations in the first Brillouin zone were made using a Monkhorst–Pack[51] grid of 3×3×1 k-points. All the calculations were performed at the non-spin-polarized level, however, the spin-polarized level was considered for the adsorption on the monovacancy.

In order to represent the (van der Waals) dominant inverse sixth-power dependence of the interaction energy on inter-fragment distance *R*, due to nonlocal correlation electronic effects missing in standard DFT, three main approaches have been previously suggested.[52] One consists of the implementation of conventional exchange and correlation functionals in the GGA according to hybrid or *meta*-hybrid schemes (see, for example, Ref. [53]). In another approach, the way to take into account the dispersion interaction is the inclusion of a pairwise parametrized term with an inverse sixth-power dependence on interfragment distance to the total energy obtained in standard DFT.[54] In contrast, in the third type of method, a nonlocal self-consistent correlation energy term is added to the exchange and local correlation energy terms[55] to calculate the full exchange-correlation functional of the molecular system. In the calculations performed for the present work, the vdW-like dispersive interactions were taken into account using the latter two approaches: the DFT-D2 method of Grimme et al.[56] and the vdW-DF2 method of Lundqvist and Langreth et al.,[31] corresponding to the second and third types described above, respectively. In the first method, electron exchange-correlation effects are described by the GGA approximation using the Perdew–Burke–Ernzerhof (PBE) functional.[57] In the second method, the exchange PW86 functional[58] and the local density approximation were used as exchange and local correlation contributions to the full exchange-correlation functional, respectively. It should be noted that in earlier DFT calculations for the adsorption of aromatic molecules on carbon nanosystems, the local density approximation was used to account for the electronic exchange and correlation energy,[59] giving reasonable molecule–substrate distances unlike the standard GGA approximation, with which weakened binding and overestimated molecule–substrate distances were found.

The coordinates of the adsorbed DA molecule and all the carbon atoms of the DA–G or DA–GV systems were allowed to relax until the residual Hellmann–Feynman forces were less than 0.02 eV Å^{-1}. The interaction energy between DA and the carbonaceous surface (G or GV) was calculated in terms of the adsorption energy defined as [Eq. (1)]:

$$E_{ads} = E_{DA-Surf} - E_{Surf} - E_{DA} \quad (1)$$

In this expression, $E_{DA-Surf}$ is the total energy of DA–G or DA–GV systems, E_{DA} is the energy of the isolated DA molecule, and E_{Surf} is the total energy of the clean DA–G or DA–GV systems. In this way, negative values for E_{ads} correspond to exothermic processes.

The analysis of charge reorganization due to adsorption was accomplished by calculating the electronic charge density difference, $\Delta\rho$, produced as a consequence of the adsorption process. This electronic property can be expressed as [Eq. (2)]:

$$\Delta\rho = \rho_{DA-Surf} - \rho_{Surf} - \rho_{DA} \quad (2)$$

where $\rho_{DA-Surf}$ in the charge density of the total DA–G or DA–GV systems, ρ_{Surf} is the charge density of the graphene substrate and ρ_{DA} is the density of the DA molecule, the latter two charge densities were calculated as isolated fragments but with the same geometry as for DA adsorbed on graphene or GV surfaces. The electronic structure was analyzed by computing the PDOS on selected atoms of the adsorbate and substrate. For that purpose, a grid of $11\times11\times1$ k-points was used.

The noncovalent interactions between adsorbate and substrate were analyzed by means of the NCI,[45] as implemented in the latest version of Critic code.[60] The NCI is based on a 2D plot of the reduced density gradient, s, and the electron density, ρ, where [Eq. (3)]:

$$s = \frac{1}{2(3\pi^2)^{\frac{1}{3}}} \frac{|\nabla\rho|}{\rho^{4/3}} \quad (3)$$

If noncovalent interactions are present in a system, steep peaks appear at low densities in this 2D plot. However, the sign and magnitude of λ_2, the second-largest eigenvalue of the electron-density Hessian matrix, allows the nature of this interaction to be known. Then, the 3D plotting of sign$(\lambda_2)\rho$ on an isosurface of the reduced density gradient allows regions of different noncovalent nature to be defined. The plotting of 3D isosurfaces for the $\Delta\rho$ function was performed using the VESTA3 code[61] and the VMD code was used for the NCI.[62]

Regarding the calculations to evaluate the solvent effect, the PBE functional[57] and the polarized continuum model (PCM)[63] were used with the 6-31++G(d,p) basis set as implemented in the Gaussian 03 package.[64]

Acknowledgements

The authors want to acknowledge financial support from these Argentine institutions: Consejo Nacional de Investigaciones Científicas y Técnicas, Agencia Nacional de Promoción Científica y Tecnológica and Universidad Nacional del Sur, under Grants PIP No. 112-200801-02286, PICT-2014-1778 and PGI 24/F063, respectively.

Conflict of Interest

The authors declare no conflict of interest.

Keywords: adsorption · density functional calculations · dopamine · graphene · monovacancies

[1] R. A. Potyrailo, C. Surman, N. Nagraj, A. Burns, *Chem. Rev.* **2011**, *111*, 7315–7354.
[2] F. Schedin, A. K. Geim, S. V. Morozov, E. W. Hill, P. Blake, M. I. Katsnelson, K. S. Novoselov, *Nat. Mater.* **2007**, *6*, 652–655.
[3] R. Stine, S. P. Mulvaney, J. T. Robinson, C. R. Tamanaha, P. E. Sheehan, *Anal. Chem.* **2013**, *85*, 509–552.
[4] W. Lin, B. Tian, P. Zhuang, J. Yin, C. Zhang, Q. Li, T.-M. Shih, W. Cai, *Nano Lett.* **2016**, *16*, 5737–5741.
[5] S. Li, A. N. Aphale, I. G. Macwan, P. K. Patra, W. G. Gonzalez, J. Miksovska, R. M. Leblanc, *ACS Appl. Mater. Interfaces* **2012**, *4*, 7069–7075.
[6] L. Tang, Y. Wang, Y. Li, H. Feng, J. Lu, J. Li, *Adv. Funct. Mater.* **2009**, *19*, 2782–2789.
[7] Y. Shao, J. Wang, H. Wu, J. Liu, I. A. Aksay, Y. Lin, *Electroanalysis* **2010**, *22*, 1027–1036.
[8] D. Chen, L. Tang, J. Li, *Chem. Soc. Rev.* **2010**, *39*, 3157–3180.
[9] Y.-H. Zhang, Y.-B. Chen, K.-G. Zhou, C.-H. Liu, J. Zeng, H.-L. Zhang, Y. Peng, *Nanotechnology* **2009**, *20*, 185504.
[10] M. L. A. V. Heien, A. S. Khan, J. L. Ariansen, J. F. Cheer, P. E. M. Phillips, K. M. Wassum, R. M. Wightman, *Proc. Natl. Acad. Sci. USA* **2005**, *102*, 10023–10028.
[11] J. Birtwistle, D. Baldwin, *Br. J. Nurs.* **1998**, *7*, 832–841.
[12] Y. Wang, Y. Li, L. Tang, J. Lu, J. Li, *Electrochem. Commun.* **2009**, *11*, 889–892.
[13] Y.-R. Kim, S. Bong, Y.-J. Kang, Y. Yang, R. K. Mahajan, J. S. Kim, H. Kim, *Biosens. Bioelectron.* **2010**, *25*, 2366–2369.
[14] L. Wu, L. Feng, J. Ren, X. Qu, *Biosens. Bioelectron.* **2012**, *34*, 57–62.
[15] M. Zhang, C. Liao, Y. Yao, Z. Liu, F. Gong, F. Yan, *Adv. Funct. Mater.* **2014**, *24*, 978–985.
[16] M. M. Sari, *Mater. Chem. Phys.* **2013**, *138*, 843–849.
[17] S. Grimme, *Angew. Chem. Int. Ed.* **2008**, *47*, 3430–3434; *Angew. Chem.* **2008**, *120*, 3478–3483.
[18] S. Gowtham, R. H. Scheicher, R. Pandey, S. P. Karna, R. Ahuja, *Nanotechnology* **2008**, *19*, 125701.
[19] D. Le, A. Kara, E. Schröder, P. Hyldgaard, T. S. Rahman, *J. Phys. Condens. Matter* **2012**, *24*, 424210.
[20] H. Vovusha, S. Sanyal, B. Sanyal, *J. Phys. Chem. Lett.* **2013**, *4*, 3710–3718.
[21] X. Sun, Z. Liu, K. Welsher, J. T. Robinson, A. Goodwin, S. Zaric, H. Dai, *Nano Res.* **2008**, *1*, 203–212.
[22] Z. Liu, J. T. Robinson, X. Sun, H. Dai, *J. Am. Chem. Soc.* **2008**, *130*, 10876–10877.
[23] D. Umadevi, S. Panigrahi, G. N. Sastry, *Acc. Chem. Res.* **2014**, *47*, 2574–2581.
[24] M. Chourasia, G. M. Sastry, G. N. Sastry, *Int. J. Biol. Macromol.* **2011**, *48*, 540–552.
[25] S. Panigrahi, A. Bhattacharya, S. Banerjee, D. Bhattacharyya, *J. Phys. Chem. C* **2012**, *116*, 4374–4379.
[26] A. Rochefort, J. D. Wuest, *Langmuir* **2009**, *25*, 210–215.
[27] W. Qin, X. Li, W.-W. Bian, X.-J. Fan, J.-Y. Qi, *Biomaterials* **2010**, *31*, 1007–1016.
[28] K. Yan, H. Peng, Y. Zhou, H. Li, Z. Liu, *Nano Lett.* **2011**, *11*, 1106–1110.
[29] M. Birowska, K. Milowska, J. A. Majewski, *Acta Phys. Pol. A* **2011**, *120*, 845–848.
[30] Y. X. Zhao, I. L. Spain, *Phys. Rev. B* **1989**, *40*, 993–997.
[31] K. Lee, É. D. Murray, L. Kong, B. I. Lundqvist, D. C. Langreth, *Phys. Rev. B* **2010**, *82*, 081101.
[32] J. Ortiz-Medina, F. López-Urías, H. Terrones, F. J. Rodríguez-Macías, M. Endo, M. Terrones, *J. Phys. Chem. C* **2015**, *119*, 13972–13978.
[33] D. Umadevi, G. N. Sastry, *J. Phys. Chem. Lett.* **2011**, *2*, 1572–1576.
[34] S. Gowtham, R. H. Scheicher, R. Ahuja, R. Pandey, S. P. Karna, *Phys. Rev. B* **2007**, *76*, 2–5.
[35] F. Ortmann, W. G. Schmidt, F. Bechstedt, *Phys. Rev. Lett.* **2005**, *95*, 1–4.

[36] C. Fonseca Guerra, J. W. Handgraaf, E. J. Baerends, F. M. Bickelhaupt, *J. Comput. Chem.* **2004**, *25*, 189 – 210.
[37] O. Leenaerts, B. Partoens, F. M. Peeters, *Phys. Rev. B* **2008**, *77*, 125416.
[38] J. Antony, S. Grimme, *Phys. Chem. Chem. Phys.* **2008**, *10*, 2722 – 2729.
[39] D. Cortés-Arriagada, A. Toro-Labbé, *Phys. Chem. Chem. Phys.* **2015**, *17*, 12056 – 12064.
[40] N. F. Domancich, R. M. Ferullo, N. J. Castellani, *J. Theor. Comput. Chem.* **2014**, *13*, 1450055.
[41] R. Singh, P. Kroll, *J. Phys. Condens. Matter* **2009**, *21*, 196002.
[42] George A. Jeffrey, *An Introduction to Hydrogen Bonding*, Oxford University Press, New York, **1997**, Chap. 2.
[43] N. F. Domancich, R. M. Ferullo, N. J. Castellani, *Comput. Theor. Chem.* **2015**, *1059*, 27 – 34.
[44] G. A. DiLabio, A. Otero-de-la-Roza in *Reviews in Computational Chemistry, Vol. 29* (Eds.: A. L. Parrill, K. B. Lipkowitz), Wiley, Hoboken, **2016**, Chap. 1.
[45] E. R. Johnson, S. Keinan, P. Mori-Sánchez, J. Contreras-García, A. J. Cohen, W. Yang, *J. Am. Chem. Soc.* **2010**, *132*, 6498 – 6506.
[46] I. Fampiou, A. Ramasubramaniam, *J. Phys. Chem. C* **2012**, *116*, 6543 – 6555.
[47] G. Kresse, J. Furthmüller, *Phys. Rev. B* **1996**, *54*, 11169 – 11186.
[48] G. Kresse, J. Furthmüller, *Comput. Mater. Sci.* **1996**, *6*, 15 – 50.
[49] P. E. Blöchl, *Phys. Rev. B* **1994**, *50*, 17953 – 17979.
[50] G. Kresse, D. Joubert, *Phys. Rev. B* **1999**, *59*, 1758 – 1775.
[51] H. J. Monkhorst, J. D. Pack, *Phys. Rev. B* **1976**, *13*, 5188 – 5192.
[52] S. Grimme, J. Antony, T. Schwabe, C. Mück-Lichtenfeld, *Org. Biomol. Chem.* **2007**, *5*, 741 – 758.
[53] Y. Zhao, D. G. Truhlar, *Acc. Chem. Res.* **2008**, *41*, 157 – 167.
[54] S. Grimme, *J. Comput. Chem.* **2006**, *27*, 1787 – 1799.
[55] M. Dion, H. Rydberg, E. Schröder, D. C. Langreth, B. I. Lundqvist, *Phys. Rev. Lett.* **2004**, *92*, 246401.
[56] S. Grimme, J. Antony, S. Ehrlich, H. Krieg, *J. Chem. Phys.* **2010**, *132*, 154104.
[57] J. P. Perdew, K. Burke, M. Ernzerhof, *Phys. Rev. Lett.* **1996**, *77*, 3865 – 3868.
[58] J. P. Perdew, W. Yue, *Phys. Rev. B* **1986**, *33*, 8800 – 8802.
[59] F. Tournus, S. Latil, M.. Heggie, J.-C. Charlier, *Phys. Rev. B* **2005**, *72*, 75431.
[60] A. Otero-de-la-Roza, E. R. Johnson, J. Contreras-García, *Phys. Chem. Chem. Phys.* **2012**, *14*, 12165.
[61] K. Momma, F. Izumi, *J. Appl. Crystallogr.* **2011**, *44*, 1272 – 1276.
[62] a) W. Humphrey, A. Dalke, K. Schulten, *J. Mol. Graphics* **1996**, *14*, 33 – 38; b) http://www.ks.uiuc.edu/Research/vmd/.
[63] S. Miertuš, J. Tomasi, *Chem. Phys.* **1982**, *65*, 239 – 245.
[64] *Gaussian 03 (Revision D.01)*, M. J. Frisch, G. W. Trucks, H. B. Schlegel, G. E. Scuseria, M. A. Robb, J. R. Cheeseman, J. A. Montgomery, Jr., T. Vreven, K. N. Kudin, J. C. Burant, J. M. Millam, S. S. Iyengar, J. Tomasi, V. Barone, B. Mennucci, M. Cossi, G. Scalmani, N. Rega, G. A. Petersson, H. Nakatsuji, M. Hada, M. Ehara, K. Toyota, R. Fukuda, J. Hasegawa, M. Ishida, T. Nakajima, Y. Honda, O. Kitao, H. Nakai, M. Klene, X. Li, J. E. Knox, H. P. Hratchian, J. B. Cross, V. Bakken, C. Adamo, J. Jaramillo, R. Gomperts, R. E. Stratmann, O. Yazyev, A. J. Austin, R. Cammi, C. Pomelli, J. W. Ochterski, P. Y. Ayala, K. Morokuma, G. A. Voth, P. Salvador, J. J. Dannenberg, V. G. Zakrzewski, S. Dapprich, A. D. Daniels, M. C. Strain, O. Farkas, D. K. Malick, A. D. Rabuck, K. Raghavachari, J. B. Foresman, J. V. Ortiz, Q. Cui, A. G. Baboul, S. Clifford, J. Cioslowski, B. B. Stefanov, G. Liu, A. Liashenko, P. Piskorz, I. Komaromi, R. L. Martin, D. J. Fox, T. Keith, M. A. Al-Laham, C. Y. Peng, A. Nanayakkara, M. Challacombe, P. M. W. Gill, B. Johnson, W. Chen, M. W. Wong, C. Gonzalez, J. A. Pople, Gaussian, Inc., Wallingford, CT, **2004**.

Manuscript received: March 10, 2017
Revised manuscript received: May 10, 2017
Accepted manuscript online: May 11, 2017
Version of record online: ■■ ■■, 0000

ARTICLES

Perfectly noncovalent! The adsorption of dopamine on perfect graphene involves noncovalent interactions of π–π and CH···π character, according to the adsorption mode, as well as electron drift from substrate to adsorbate. On graphene with monovacancies, a hydrogen bond is formed involving a hydroxy group of dopamine and a carbon atom of the vacancy in the AB stacking mode.

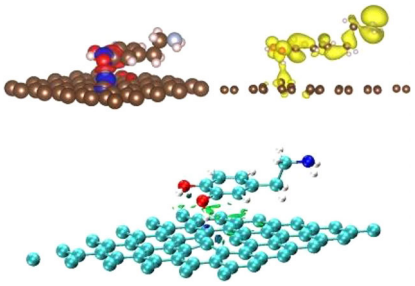

*A. C. R. Fernández, N. J. Castellani**

■■ – ■■

Noncovalent Interactions between Dopamine and Regular and Defective Graphene